J. Inverse Ill-Posed Probl., Ahead of Print
DOI 10.1515/jip-2013-0042

Reconstructing conductivities with boundary corrected D-bar method

Samuli Siltanen and Janne P. Tamminen

Abstract. The aim of electrical impedance tomography is to form an image of the conductivity distribution inside an unknown body using electric boundary measurements. The computation of the image from measurement data is a non-linear ill-posed inverse problem and calls for a special regularized algorithm. One such algorithm, the so-called D-bar method, is improved in this work by introducing new computational steps that remove the so far necessary requirement that the conductivity should be constant near the boundary. The numerical experiments presented suggest two conclusions. First, for most conductivities arising in medical imaging, it seems the previous approach of using a best possible constant near the boundary is sufficient. Second, for conductivities that have high contrast features at the boundary, the new approach produces reconstructions with smaller quantitative error and with better visual quality.

Keywords. Inverse problem, ill-posed problem, electrical impedance tomography, inverse conductivity problem.

2010 Mathematics Subject Classification. Primary 58F15, 58F17; secondary 53C35.

1 Introduction

The aim of electrical impedance tomography (EIT) is to form an image of the conductivity distribution inside an unknown body using electric boundary measurements. Applications of EIT include medical imaging, nondestructive testing and subsurface monitoring. See [16] for an overview of EIT. The computation of the image from measurement data is a non-linear ill-posed inverse problem and calls for a special regularized algorithm. In this work we improve one such algorithm, the so-called D-bar method, by removing the so far necessary requirement that the conductivity should be constant near the boundary.

The mathematical model behind EIT is the *inverse conductivity problem* introduced by Calderón in [14]. We discuss here the inverse conductivity problem in

The second author was supported by Tampere University of Technology and Pirkanmaan kulttuurirahasto. The research work of both authors was funded in part by the Finnish Centre of Excellence in Inverse Problems Research (Academy of Finland CoE-project 213476).

the following two-dimensional form: let $\Omega_1 = D(0, r_1) \subset \mathbb{R}^2$ be the disc with center at origin and radius $r_1 > 0$ and consider a strictly positive, real-valued conductivity $\sigma \in C^2(\overline{\Omega_1})$. Maintaining a voltage distribution f on the boundary $\partial\Omega_1$ creates a voltage potential u that solves the following Dirichlet problem:

$$\begin{cases} \nabla \cdot (\sigma \nabla u) = 0 & \text{in } \Omega_1, \\ u = f & \text{on } \partial\Omega_1. \end{cases} \tag{1.1}$$

The resulting distribution of current through the boundary is

$$\Lambda_\sigma f = \sigma \frac{\partial u}{\partial \nu}\Big|_{\partial\Omega_1}, \tag{1.2}$$

where ν is the outward unit normal and Λ_σ is the Dirichlet-to-Neumann (DN) map. Calderón's problem is to reconstruct σ from the knowledge of Λ_σ.

Many numerical methods have been suggested in the literature for the reconstruction of σ in the above setting. In this work we concentrate on the so-called D-bar method. Other approaches include linearization [5, 8, 17], iterative regularization [20, 21, 27, 38], statistical inversion [26, 49], resistor network methods [11], convexification [51], layer stripping [53, 54], Teichmüller space methods [35–37]. Also, there is a large body of work concentrating on recovering partial information on σ, see [9, 10] for a survey.

The D-bar method considered in this paper is the implementation of Nachman's constructive proof [43] for recovering $\sigma \in W^{2,p}(\Omega_1)$ from Λ_σ for $p > 1$. That result builds on the previous work of Sylvester and Uhlmann 1987 [55] and Nachman 1988 [42] in dimensions $n \geq 3$ and on the work of Novikov 1988 [45] in dimensions $n \geq 2$. Nachman's result was later sharpened by Brown and Uhlmann in [13] to cover $W^{1,q}(\Omega_1)$ conductivities with $q > 2$; the proof was augmented with constructive steps by Knudsen and Tamasan in [34]. Finally, Astala and Päivärinta answered Calderón's question in its original form by describing a constructive procedure for recovering $\sigma \in L^\infty(\Omega_1)$ in [3, 4]; numerical implementation of this approach is described in [1, 2]. Thus there are several variants of the D-bar method for two-dimensional EIT. In dimension three the theory in a more general setting of inverse scattering is developed in [45–48] and specifically the theory of three-dimensional D-bar for EIT in [7, 19, 42, 55].

The above theoretical results on the D-bar method assume the knowledge of the infinite-precision data Λ_σ. However, the starting point of practical inversion is a finite-dimensional and noisy approximation L_σ^ε to Λ_σ. Since the EIT problem is severely ill-posed, or sensitive to measurement noise, any practical reconstruction method needs to be robust against errors in measurement data. The first robust D-bar algorithm (based on [43]) was given in [52], and it has been refined and

analyzed in [30, 31, 33, 39]. The method has been successfully tested on a chest phantom in [24] and on *in vivo* human chest data in [25]. Numerical D-bar method based on [13, 34] was reported in [29]. The above methods are two-dimensional; three-dimensional computations are described in [6, 12]. Robustness is ensured in all of these practical D-bar reconstruction methods by truncating scattering data, a step that can be viewed as nonlinear low-pass filtering.

In addition to being robust against noise, a reliable EIT algorithm needs a regularization analysis. Such an analysis is provided for the two-dimensional D-bar method in [32], where an explicit formula is given for choosing the truncation radius as function of noise level.

Practical D-bar methods have been until now implemented by fitting an optimal constant to the possibly nonconstant trace $\sigma|_{\partial\Omega_1}$. Quite good results have been obtained both with laboratory data [24] and *in vivo* patient data [25]. However, in applications exhibiting large conductivity changes near or at the boundary the constant-fitting approach may not be good enough. Our aim here is to remove the assumption "$\sigma \equiv 1$ near the boundary" from the two-dimensional D-bar algorithm based on [43] using an additional procedure we call *boundary correction*.

Let us review the infinite-precision boundary correction procedure given in [43]. The starting point is the DN map Λ_σ of a conductivity $\sigma \in W^{2,p}(\Omega_1)$. Take $r_2 > r_1$ and set $\Omega_2 = D(0, r_2)$. The conductivity σ is extended outside Ω_1 by

$$\gamma(x) = \begin{cases} \sigma(x), & \text{when } x \in \Omega_1, \\ \tilde{\sigma}(x), & \text{when } x \in \Omega_2 \setminus \overline{\Omega_1}, \end{cases} \tag{1.3}$$

where we can choose any $\tilde{\sigma} \in W^{2,p}(\Omega_2 \setminus \overline{\Omega_1})$ with the properties $\tilde{\sigma}|_{\partial\Omega_1} = \sigma|_{\partial\Omega_1}$ and $(\partial\sigma/\partial\nu)|_{\partial\Omega_1} = (\partial\tilde{\sigma}/\partial\nu)|_{\partial\Omega_1}$ and $\tilde{\sigma} \equiv 1$ near $\partial\Omega_2$. This way $\gamma \in W^{2,p}(\Omega_2)$ whenever $\sigma \in W^{2,p}(\Omega_1)$. Define two Dirichlet problems:

$$\begin{cases} \nabla \cdot (\tilde{\sigma} \nabla u_j) = 0 & \text{in } \Omega_2 \setminus \overline{\Omega_1},\ j = 1, 2, \\ u_j = f_j & \text{on } \partial\Omega_j, \\ u_j = 0 & \text{on } \partial\Omega_i,\ i = 1, 2,\ i \neq j. \end{cases} \tag{1.4}$$

Four new DN maps in $\Omega_2 \setminus \overline{\Omega_1}$ can be defined by

$$\Lambda^{ij} f_j = \tilde{\sigma} \frac{\partial u_j}{\partial \nu}\Big|_{\partial\Omega_i}, \quad i, j = 1, 2. \tag{1.5}$$

By [43, Proposition 6.1] we can use (1.5) to write Λ_γ in terms of Λ_σ:

$$\Lambda_\gamma = \Lambda^{22} + \Lambda^{21}(\Lambda_\sigma - \Lambda^{11})^{-1}\Lambda^{12}. \tag{1.6}$$

The boundary corrected D-bar method for $\sigma \in W^{2,p}(\Omega_1)$, assuming infinite-precision data, is described as follows in [43, Section 6]:

(a) **Reconstruction at the boundary.** Recover the trace $\sigma|_{\partial\Omega_1}$ and the normal derivative $(\partial\sigma/\partial\nu)|_{\partial\Omega_1}$ from Λ_σ.

(b) **Extension of conductivity.** Using (a) and (1.3), extend the conductivity to $\gamma \in W^{2,p}(\Omega_2)$ such that $\gamma \equiv 1$ near $\partial\Omega_2$ and $\inf_{x\in\Omega_2} \gamma(x) \geq c > 0$.

(c) **Calculation of outer DN map.** Write the DN map Λ_γ of $\gamma \in W^{2,p}(\Omega_2)$ in terms of Λ_σ using (1.6).

(d) **Reconstruction using the D-bar method.** Reconstruct $\gamma \in W^{2,p}(\Omega_2)$ from the infinite-precision data Λ_γ following [43].

The practical starting point of reconstruction is the noisy approximate data L_σ^ε, and the Steps (a)–(d) above cannot be directly followed. We suggest the following robust procedure for boundary correction:

(a′) **Approximate reconstruction at the boundary.** Recover numerically a smooth function $g \in C^\infty(\partial\Omega_1)$ with the property $g \approx \sigma|_{\partial\Omega_1}$ as explained in [44]. Omit recovering $(\partial\sigma/\partial\nu)|_{\partial\Omega_1}$ since it is an unstable step [44].

(b′) **Simple extension of conductivity.** Construct $\tilde{\sigma} \in C^2(\overline{\Omega_2 \setminus \Omega_1})$ satisfying $\inf_{x\in\Omega_2\setminus\overline{\Omega_1}} \tilde{\sigma}(x) \geq c > 0$ and $\tilde{\sigma}|_{\partial\Omega_1} = g$ and $\tilde{\sigma} \equiv 1$ near $\partial\Omega_2$. Use $\tilde{\sigma}$ in (1.3) to extend the conductivity to $\gamma \in L^\infty(\Omega_2)$.

(c′) **Approximate calculation of outer DN map.** Write approximate DN map L_γ in terms of L_σ using a matrix approximation to (1.6).

(d′) **Reconstruction using regularized D-bar method.** Reconstruct γ from L_γ using the regularized D-bar method described in [32].

The main concern about the procedure (a′)–(d′) is that the extension of σ to γ will be in general discontinuous at $\partial\Omega_1$, and thus γ violates the assumptions of the D-bar method used in (d′). However, there is both theoretical and experimental evidence suggesting that the step (d′) should give reasonable results even in this case [24, 25, 30, 31]. Another potential problem arises from the inverse operator in formula (1.6), as the proof of invertibility [43, Proposition 6.1] in the extended conductivity produced by step (b′). One possibility would be to use [28, Lemma 2.1.3.] instead of (1.6) as the basis of step (b′). However, in our computational experiments the use of (1.6) seems not to be a problem even in the case of discontinuous conductivity extensions.

This paper should be viewed as a report of computational experiments suggesting the practical usefulness of the boundary correction step in applications where the conductivity varies strongly near the boundary. Hopefully the computational

results presented below will act as motivation for further theoretical study of practical imaging algorithms for EIT.

We remark that the boundary correction method is applied in this paper only in the case of Ω_1 being a disc. This is not a serious lack of generality, though: we presume that other domains than discs could be treated combining the methods described in [40, 41] with the boundary correction.

This paper is organized as follows. We present our method of simulating continuum model EIT data in Section 2. The details of implementation of Steps (a′), (b′) and (c′) are discussed in Sections 3, 4 and 5, respectively. A brief outline of the regularized D-bar method is given in Section 6. Our practical boundary correction method is illustrated by numerical examples in Section 7, and we conclude our results in Section 8.

2 Simulation of measurement data

Let $\mathcal{R}_\sigma : \widetilde{H}^{-1/2}(\partial\Omega_1) \to \widetilde{H}^{1/2}(\partial\Omega_1)$ denote the Neumann-to-Dirichlet (ND) map of σ, where $\widetilde{H}^s$ spaces consist of H^s functions with mean value zero. We have

$$\mathcal{R}_\sigma g = u|_{\partial\Omega_1},$$

where u is the unique $H^1(\Omega_1)$ solution of the Neumann problem

$$\begin{cases} \nabla \cdot \sigma \nabla u = 0 & \text{in } \Omega_1, \\ \gamma \dfrac{\partial u}{\partial \nu} = g & \text{on } \partial\Omega_1, \end{cases}$$

satisfying

$$\int_{\partial\Omega_1} u ds = 0.$$

We note two key equalities concerning Λ_σ and $\mathcal{R}_\sigma$. Define a projection operator

$$P\phi := |\partial\Omega_1|^{-1} \int_{\partial\Omega_1} \phi.$$

Then for any $f \in H^{1/2}(\partial\Omega_1)$ we have

$$P\Lambda_\sigma f = |\partial\Omega_1|^{-1} \int_{\partial\Omega_1} \sigma \frac{\partial u}{\partial \nu} = \int_{\Omega_1} \nabla \cdot \sigma \nabla u = 0,$$

so actually $\Lambda_\sigma : H^{1/2}(\partial\Omega_1) \to \widetilde{H}^{-1/2}(\partial\Omega_1)$. From the definitions of Λ_σ and $\mathcal{R}_\sigma$ we now have

$$\Lambda_\sigma \mathcal{R}_\sigma = I : \widetilde{H}^{-1/2}(\partial\Omega_1) \to \widetilde{H}^{-1/2}(\partial\Omega_1), \tag{2.1}$$

$$\mathcal{R}_\sigma \Lambda_\sigma = I - P : H^{1/2}(\partial\Omega_1) \to \widetilde{H}^{1/2}(\partial\Omega_1). \tag{2.2}$$

Given σ and $N > 0$, we define a matrix $R_\sigma : \mathbb{C}^{2N} \to \mathbb{C}^{2N}$ as follows. We use a truncated orthonormal trigonometric basis for representing functions defined at the boundary $\partial\Omega_j$:

$$\phi_j^{(n)}(\theta) = \frac{1}{\sqrt{2\pi r_j}} e^{in\theta}, \quad n = -N, \ldots, N, \ j = 1, 2. \tag{2.3}$$

Note that $\int_{\partial\Omega_j} \phi_j^{(n)} ds = 0$ for $n \neq 0$. Then solve the Neumann problem

$$\begin{cases} \nabla \cdot \sigma \nabla u_1^{(n)} = 0 & \text{in } \Omega_1, \\ \sigma \dfrac{\partial u_1^{(n)}}{\partial \nu} = \phi_1^{(n)} & \text{on } \partial\Omega_1, \end{cases} \tag{2.4}$$

with the constraint

$$\int_{\partial\Omega_1} u_1^{(n)} ds = 0.$$

Define $R_\sigma = [\widehat{u}(\ell, n)]$ by

$$\widehat{u}(\ell, n) = \int_{\partial\Omega_1} u_1^{(n)} \overline{\phi_1^{(\ell)}} ds. \tag{2.5}$$

Here ℓ is the row index and n is the column index.

The matrix R_σ represents the operator $\mathcal{R}_\sigma$ approximately. We add simulated measurement noise by defining

$$R_\sigma^\varepsilon := R_\sigma + cE, \tag{2.6}$$

where E is a $(2N \times 2N)$ matrix with random entries independently distributed according to the Gaussian normal density $\mathcal{N}(0, 1)$. The constant $c > 0$ is adjusted so that $\|R_1^\varepsilon - R_1\|/\|R_1\|$, where $\|\cdot\|$ is the standard matrix norm and R_1 is the ND map for the unit conductivity, is greater than the relative error caused by FEM and of the same order of magnitude as 0.0017 % (signal to noise -ratio of 95.5 dB), the noise level of the ACT3 impedance tomography imager of Rensselaer Polytechnic Institute [18].

We can now easily compute the corresponding noisy matrix representation L_σ^ε for the DN map Λ_σ. Namely, define

$$\widetilde{L_\sigma^\varepsilon} := (R_\sigma^\varepsilon)^{-1};$$

then $\widetilde{L_\sigma^\varepsilon}$ is a matrix of size $2N \times 2N$. We should add appropriate mapping properties for constant basis functions at the boundary according to the facts

$$\Lambda_\sigma 1 = 0, \quad \int_{\partial\Omega_1} \Lambda_\sigma f ds = 0.$$

This is achieved simply by setting (in Matlab notation)

$$L_\sigma^\varepsilon := \begin{bmatrix} \widetilde{L_\sigma^\varepsilon}(1{:}N, 1{:}N) & 0 & \widetilde{L_\sigma^\varepsilon}(1{:}N, (N+1){:}\text{end}) \\ 0 & 0 & 0 \\ \widetilde{L_\sigma^\varepsilon}((N+1){:}\text{end}, 1{:}N) & 0 & \widetilde{L_\sigma^\varepsilon}((N+1){:}\text{end}, (N+1){:}\text{end}) \end{bmatrix}, \quad (2.7)$$

where the zero block matrices above have various (but obvious) sizes.

3 Approximate reconstruction at the boundary

The trace $\sigma|_{\partial\Omega_1}$ can be approximately reconstructed in the following way [44]. Define

$$h_{M,\beta}(\theta) = e^{iM\theta}\eta(\theta - \beta),$$

where

$$\eta(\theta) = \begin{cases} d(\kappa\theta - \frac{\pi}{2})^\alpha(\kappa\theta + \frac{\pi}{2})^\alpha \cos(\kappa\theta), & \text{for } -\frac{\pi}{2\kappa} < \theta < \frac{\pi}{2\kappa}, \\ 0, & \text{otherwise,} \end{cases} \quad (3.1)$$

is a non-negative cut-off function satisfying

$$\int_{\partial\Omega_1} \eta^2(\theta)d\theta = 1.$$

Now the mollified trace $(\sigma\eta^2)|_{\partial\Omega_1}(\beta)$ can be calculated with

$$\int_{\partial\Omega_1} \sigma\eta^2 ds = \lim_{M\to\infty} \frac{1}{M} \int_{\partial\Omega_1} \overline{h_{M,\beta}}\Lambda_\sigma h_{M,\beta} ds. \quad (3.2)$$

We get the approximation $g \approx \sigma|_{\partial\Omega_1}$ by calculating (3.2) with different angles β and using a finite M on the right side of (3.2).

Another approach to reconstructing $\sigma|_{\partial\Omega_1}$ is the layer stripping method introduced in [53].

4 Simple extension of conductivity

The starting point here is a given approximation $g : \partial\Omega_1 \to \mathbb{R}$ to the trace $\sigma|_{\partial\Omega_1}$ of the conductivity $\sigma \in C^2(\overline{\Omega_1})$ of interest. The aim is to construct a strictly positive conductivity $\tilde{\sigma} : \Omega_2 \setminus \overline{\Omega_1}$ satisfying $\tilde{\sigma}|_{\partial\Omega_1} = g$ and $\tilde{\sigma} \equiv 1$ near the outer boundary $\partial\Omega_2$, and then use formula (1.3) to define γ.

We extend σ to γ using the following extension in polar coordinates:

$$\gamma(\rho,\theta) = \begin{cases} \sigma(\rho,\theta), & \rho \le r_1, \\ (g(\theta)-1)\, f_m(\rho) + 1, & r_1 < \rho \le r_e, \\ 1, & r_e < \rho \le r_2, \end{cases} \tag{4.1}$$

where $r_1 < r_e < r_2$ is some radius and $f_m(\rho) \ge 0$ is a suitable third-degree polynomial satisfying $f_m(r_1) = 1$ and $f_m(r_e) = 0$. Note that γ is twice continuously differentiable apart from possible discontinuity at $\rho = r_1$, and equals constant 1 in the annulus $r_e < \rho < r_2$.

5 Approximate calculation of outer DN map

Using the functions (2.3), a given function $f : \partial\Omega_i \to \mathbb{C}$ can be approximately represented by the vector

$$\vec{f} = [\hat{f}(-N), \hat{f}(-N+1), \ldots, \hat{f}(N-1), \hat{f}(N)]^T, \quad \hat{f}(n) = \int_{\partial\Omega_i} f\, \overline{\phi_i^{(n)}}\, ds,$$

and the DN maps Λ^{ij} can be approximated by the matrices $L^{ij} = [\widehat{g}_{ij}(\ell, n)]$ with

$$\widehat{g}_{ij}(\ell, n) = \int_{\partial\Omega_j} \tilde{\sigma} \frac{\partial u_j^{(n)}}{\partial \nu}\Big|_{\partial\Omega_i} \overline{\phi_j^{(\ell)}}\, dS, \tag{5.1}$$

where $u_j^{(n)}$ denotes the solution to (1.4) with $u_j^{(n)}|_{\partial\Omega_j} = \phi_j^{(n)}$. Again ℓ is the row index and n is the column index. Now the matrix L_γ^ε can be calculated by

$$L_\gamma^\varepsilon = L^{22} + L^{21}(L_\sigma^\varepsilon - L^{11})^{-1} L^{12}, \tag{5.2}$$

provided that the matrix $L_\sigma^\varepsilon - L^{11}$ is invertible. Formula (5.2) is a finite-dimensional approximation to (1.6).

6 Regularized D-bar method

In this section we explain how to reconstruct a conductivity γ in a regularized way from a noisy measurement matrix L_γ^ε under the assumptions $\gamma \in C^2(\overline{\Omega_2})$ and $\gamma \equiv 1$ in a neighborhood of $\partial\Omega_2$.

If we had the infinite-precision data Λ_γ at our disposal, we could follow the reconstruction procedure in [43]. First we would solve the boundary integral equation

$$\psi(\cdot, k)|_{\partial\Omega_2} = e^{ikx} - S_k(\Lambda_\gamma - \Lambda_1)\psi(\cdot, k)|_{\partial\Omega_2}, \tag{6.1}$$

in the Sobolev space $H^{1/2}(\partial\Omega_2)$ for all $k \in \mathbb{C} \setminus \{0\}$. In formula (6.1), S_k is a single-layer operator

$$(S_k\phi)(x) := \int_{\partial\Omega_2} G_k(x-y)\phi(y)ds,$$

where G_k is Faddeev's Green function, first introduced by L. D. Faddeev in [22], defined by

$$G_k(x) := e^{ikx}g_k(x), \quad g_k(x) := \frac{1}{(2\pi)^2}\int_{\mathbb{R}^2} \frac{e^{ix\cdot\xi}}{|\xi|^2 + 2k(\xi_1 + i\xi_2)}d\xi.$$

Once equation (6.1) had been solved, we would substitute the result into

$$\mathbf{t}(k) = \int_{\partial\Omega_2} e^{i\bar{k}\bar{x}}(\Lambda_\gamma - \Lambda_1)\psi(\cdot,k)ds, \tag{6.2}$$

where $\mathbf{t}$ is called the scattering transform, and Λ_1 is the DN map for the unit conductivity. Note that equation (6.1) and formula (6.2) are particular cases of formulas and equations first introduced by R. G. Novikov in [45]. For each fixed point $x \in \Omega$, we would solve the following integral formulation of the D-bar equation:

$$\mu(x,k) = 1 + \frac{1}{(2\pi)^2}\int_{\mathbb{R}^2} \frac{\mathbf{t}(k')}{(k-k')\bar{k'}} e^{i(k'x+\overline{k'x})}\overline{\mu(x,k')}dk'_1dk'_2. \tag{6.3}$$

Then the conductivity would be perfectly reconstructed as $\gamma(x) = \mu(x,0)^2$.

However, since our starting point in practice is the matrix L^ε_γ, we need to regularize the above ideal approach as explained in [32]. The matrices L^ε_γ and L_1 we already have, and a matrix representation $\mathbf{S}_k$ for the single-layer operator S_k can be computed numerically, provided we have numerical evaluation routines for $g_k(x)$, see [23]. We expand $e^{ikx}|_{\partial\Omega_2}$ as a vector $\vec{g}$ in our finite trigonometric basis (2.3) and set

$$\vec{\psi}_k := [I + \mathbf{S}_k(L^\varepsilon_\gamma - L_1)]^{-1}\vec{g} \tag{6.4}$$

for k ranging in a fine grid inside the disc $|k| < R$, where the truncation radius $R > 0$ is ideally chosen according to the size of noise. The choice of R falls outside the scope of this paper, so we will compute below reconstructions with R ranging in an interval. We define the truncated scattering transform by

$$\mathbf{t}_R(k) = \begin{cases} \int_{\partial\Omega_2} e^{i\bar{k}\bar{x}}\mathcal{F}^{-1}((L^\varepsilon_\gamma - L_1)\vec{\psi}_k)(x)ds, & \text{for } |k| < R, \\ 0, & \text{otherwise,} \end{cases} \tag{6.5}$$

where $\mathcal{F}^{-1}$ denotes transforming from the Fourier series domain to the function domain. Finally we use the numerical algorithm in [33] to solve equation (6.3) with $\mathbf{t}$ replaced by $\mathbf{t}_R$ and denote the solution by $\mu_R(x,k)$. Then $\gamma(x) \approx \mu_R(x,0)^2$.

7 Numerical results

We define several conductivity distributions $\sigma \in L^\infty$ on the unit disc

$$\Omega_1 = D(0, r_1) = D(0, 1)$$

and compare reconstructions computed with and without the boundary correction procedure.

Before proceeding with the examples, though, we need to choose an optimal radius r_2 to be used in the boundary correction step. We do this by examining numerically the simple case of the unit conductivity $\sigma \equiv 1$ and using the procedure (a′-c′) explained in the introduction. The numerical parameters used in this procedure are the same as in the example reconstructions, and they are given later in this chapter.

We take $N = 16$ and simulate non-noisy ND map R_1 using the finite element method with 1,048,576 triangles in Ω_1 as explained in Section 2. Using the standard square norm for matrices, this yields

$$\varepsilon_{\text{fem}} = \frac{\|R_1^{\text{th}} - R_1\|}{\|R_1^{\text{th}}\|} = 0.0000173,$$

where R_1^{th} is the analytically calculated ND matrix for the unit conductivity. Furthermore, we construct noisy ND map R_1^ε with formula (2.6) and $c = 0.00001$, giving

$$\frac{\|R_1^\varepsilon - R_1\|}{\|R_1\|} = 0.0001 > \varepsilon_{\text{fem}}.$$

To avoid notational clashes, we denote by

- $L^\varepsilon_{\gamma=1}$ the DN map on $\partial\Omega_2$ computed from noisy ND map using formula (5.2),
- $L_{\gamma=1}$ the DN map computed from non-noisy ND map using formula (5.2),
- $L^2_{\gamma=1}$ the DN map computed directly on $\partial\Omega_2$,

where by $\gamma = 1$ we mean the conductivity $\sigma = 1$ extended by (4.1). The left plot in Figure 1 shows the behavior of the error $\|L^\varepsilon_{\gamma=1} - L^2_{\gamma=1}\|/\|L^2_{\gamma=1}\|$ as function of r_2. The condition number of the matrix $L^\varepsilon_{\sigma=1} - L^{11}$ ranges between 1 and 20. It seems that we should choose $r_2 \geq 1.2$. Further, the right plot in Figure 1 shows the behavior of the error $\|L^\varepsilon_{\gamma=1} - L_{\gamma=1}\|/\|L_{\gamma=1}\|$ as function of r_2. The error decreases as r_2 grows; it shows how the data measured on $\partial\Omega_1$ contributes less and less to $L^\varepsilon_{\gamma=1}$ as r_2 gets larger. This is in agreement with the known fact that in EIT it is more difficult to obtain information from the deeper parts of the object [15].

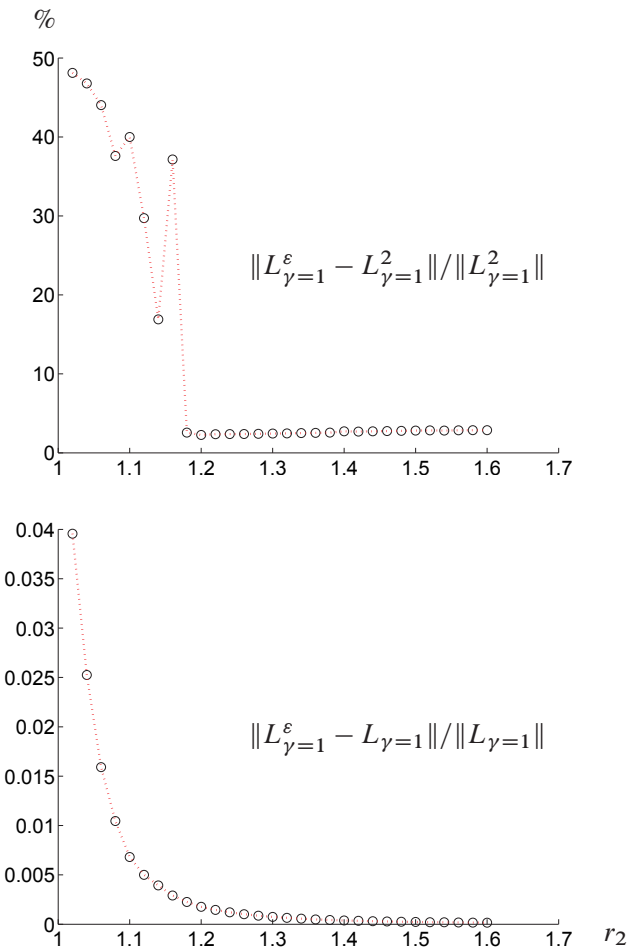

Figure 1. Top figure: relative error $\|L^{\varepsilon}_{\gamma=1} - L^{2}_{\gamma=1}\|/\|L^{2}_{\gamma=1}\|$ as a function of r_2. Here $L^{\varepsilon}_{\gamma=1}$ is the DN map on $\partial\Omega_2$ computed from noisy ND map using formula (5.2) and $L^{2}_{\gamma=1}$ is the DN map calculated directly on $\partial\Omega_2$. Here $\|\cdot\|$ denotes the standard square norm for matrices. By $\gamma = 1$ we mean $\sigma = 1$ extended by (4.1). Bottom figure: relative error $\|L^{\varepsilon}_{\gamma=1} - L_{\gamma=1}\|/\|L_{\gamma=1}\|$ as a function of r_2. Here $L_{\gamma=1}$ is the DN map computed from non-noisy ND map using formula (5.2).

Based on the above numerical investigation we choose $r_2 = 1.2$ for the rest of this paper. We work with the following four example conductivities:

- Example 1: conductivity has a high contrast bump right on the boundary $\partial\Omega_1$ and a circular inclusion near the boundary. All deviations from background conductivity 1 satisfy $\sigma(x) > 1$.
- Example 2: similar to Example 1 but with a larger inclusion having higher conductivity.
- Example 3: conductivity has high-contrast behavior near $\partial\Omega_1$, but the maximum of the deviation from background is not right at the boundary.
- Example 4: crude model of a cross-section of an industrial pipeline, similar to the case in [50]. There is a sediment layer on the bottom of the tube, and two round low-conductivity inclusions.

See Figure 2 for plots of the example conductivities and their traces on $\partial\Omega_1$.

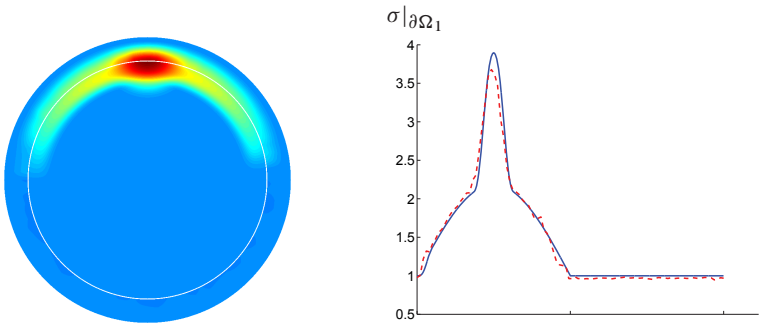

Example 1

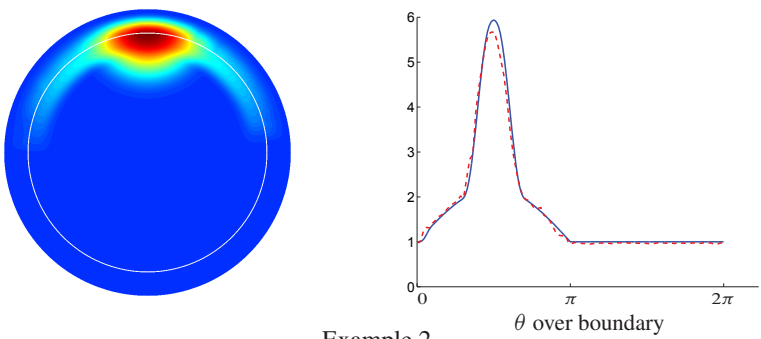

Example 2

Figure 2 (to be continued on next page)

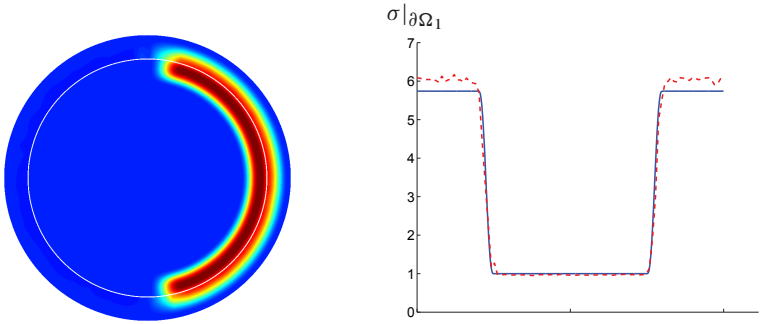

Example 3

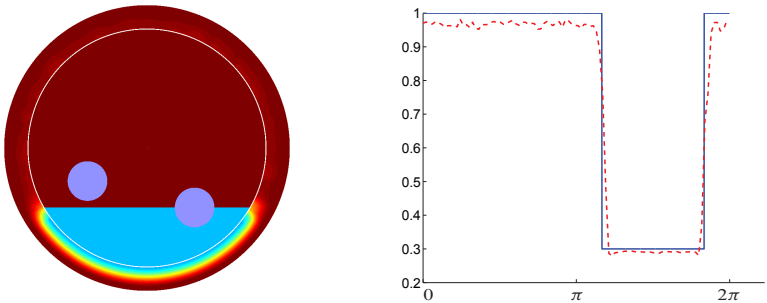

Example 4

Figure 2. Left column: Example conductivities γ shown in the extended domain Ω_2, the white circle indicates the inner boundary $\partial\Omega_1$. Right column: actual traces of the conductivities at the inner boundary $\partial\Omega_1$ (solid line), and approximate traces at $\partial\Omega_1$ (dashed line) whose reconstruction is explained in Section 3.

We simulate noisy EIT data for each example conductivity using $c = 0.00001$. The error $\|R_\sigma^\varepsilon - R_\sigma\|/\|R_\sigma\|$ ranges between 0.00011 and 0.00076.

We use the method of Section 3 with $M = 32, \kappa = 6, \alpha = 4$ and 100 different angles to compute approximately reconstructed traces g on $\partial\Omega_1$. See the right column of Figure 2 for the result. Then, we compute the extended conductivity γ in the disc $\Omega_2 = D(0, r_2) = D(0, 1.2)$ using (4.1) and (1.3) with the radius $r_e = r_1 + 7/8(r_2 - r_1) = 1.175$. Since g is only approximately the same as $\sigma|_{\partial\Omega_1}$, there are discontinuities in γ in all cases.

We compute the intermediate DN maps Λ^{ij} using the finite element method and 425,984 triangles in the annulus $\Omega_2 \setminus \overline{\Omega_1}$. To check the accuracy of formula (5.2) we also calculate Λ_γ directly by the finite element method (and 1,081,344 triangles in Ω_2) using the knowledge of γ. The error $\|L_\gamma^\varepsilon - L_\gamma^2\|/\|L_\gamma^2\|$, where L_γ^2 is

the DN map calculated directly on the boundary $\partial\Omega_2$, was less than 2.2 % in all cases. The condition number of the matrix $L_\sigma^\varepsilon - L^{11}$ used in (5.2) was less than 27 in all test cases.

Figure 3 illustrates how the noise and the boundary correction procedure affect the scattering transform in Example 4. The first row shows the real and imaginary parts of (6.5) substituting L_σ in place of $\mathcal{L}_\sigma^\varepsilon$. The second row shows the same functions using L_σ^ε, and the third row is again the same, but uses L_γ^ε calculated from (5.2). The real part of $\mathbf{t}_R(k)$ is in the left column, the imaginary part on the right. The scattering transform is calculated in a grid of spectral parameters k, where $|k| < 10$. In white areas we have $|\mathbf{t}_R(k)| > 15$, meaning the calculation has failed or is close to failing due to computational error caused by large values of $|k|$.

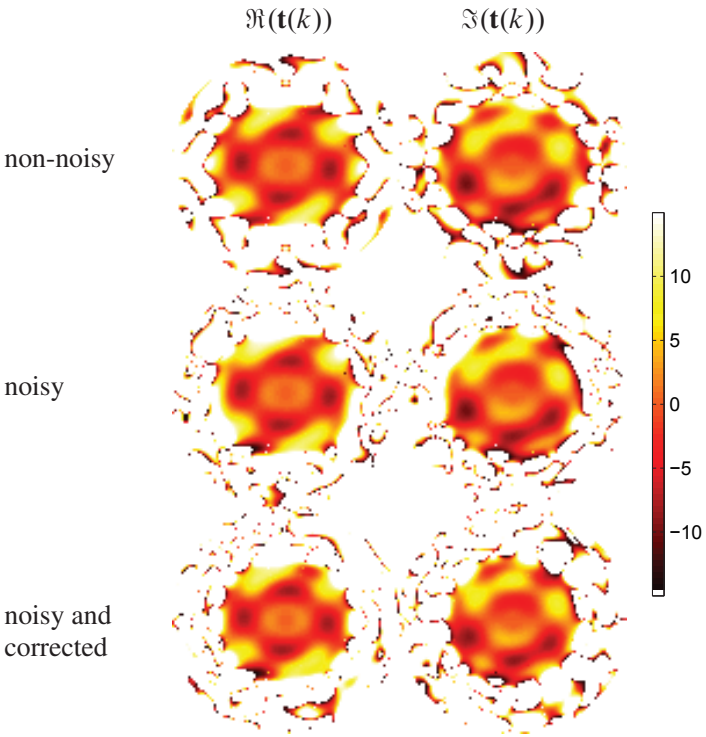

Figure 3. The scattering transform in Example 4. The first row shows the real and imaginary parts of (6.5) substituting L_σ in place of $\mathcal{L}_\sigma^\varepsilon$. The second row shows the same functions using L_σ^ε, and the third row is again the same, but uses L_γ^ε calculated from (5.2). The real part of $\mathbf{t}_R(k)$ is in the left column, the imaginary part on the right. The scattering transform is calculated in a grid of spectral parameters k, where $|k| < 10$. In white areas we have $|\mathbf{t}_R(k)| > 15$, meaning the calculation has failed or is close to failing due to computational error caused by large values of $|k|$.

For all truncation radii $R = 3.0, 3.2, \ldots, 5.8, 6.0$, as explained in Section 6, a reconstruction is calculated with and without the boundary correction procedure using the same reconstruction points. The conductivities and their extensions are pictured in Figure 2. Full error graph showing $\mathcal{L}^2$ -error for every reconstruction is pictured in Figure 4. Reconstructions and the corresponding errors are pictured in Figures 5, 6, 7 and 8. The first reconstruction pair is always calculated with $R = 3$, the second one is the one with the lowest numerical $\mathcal{L}^2$-error for the boundary corrected reconstruction, and the third one is with $R = 6$ to show how the reconstructions fail.

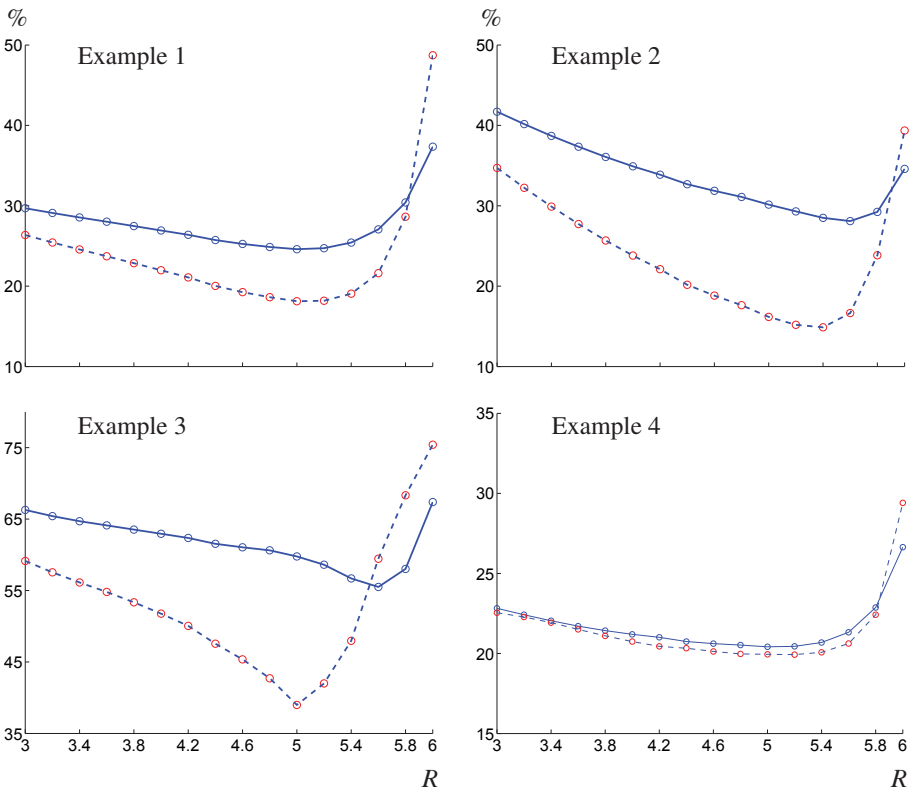

Figure 4. L^2-error graphs as a function of truncation radius R of the scattering transform for different examples; solid line is for the traditional D-bar reconstructions, dashed line is for boundary corrected reconstructions. The R-axis is the same in all four plots.

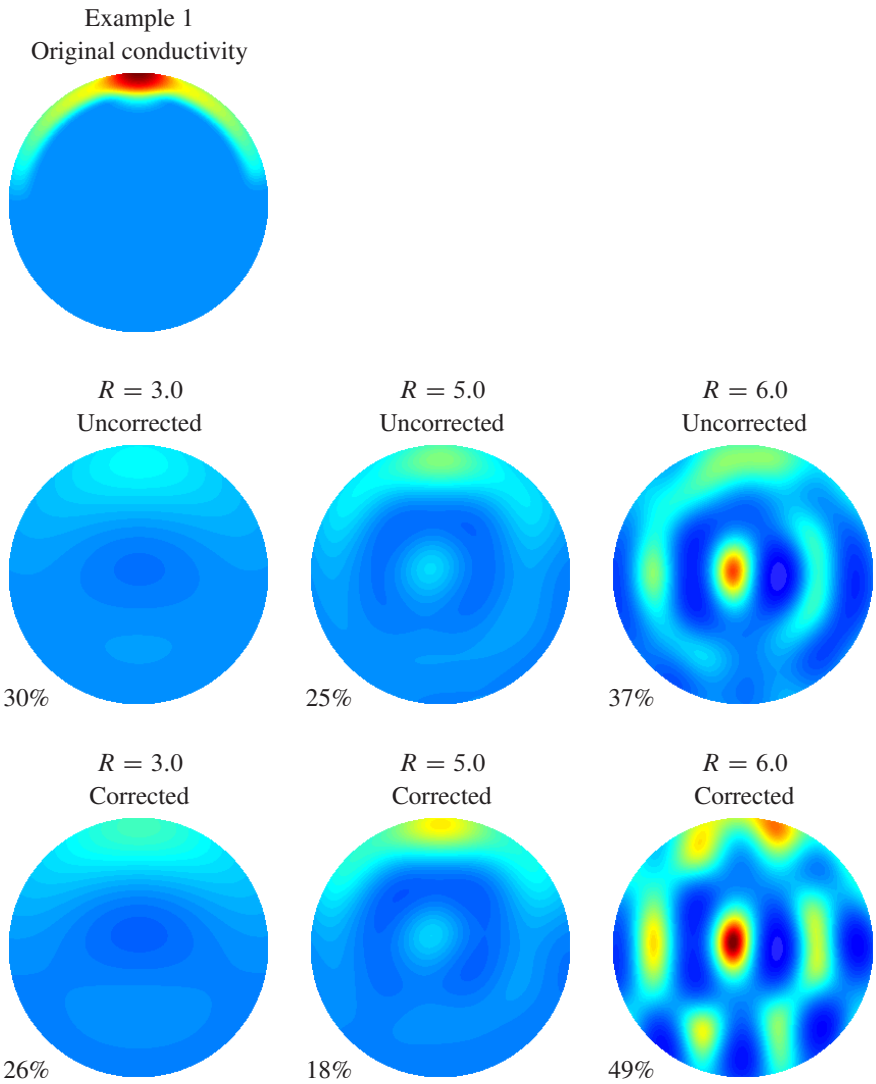

Figure 5. Example 1 reconstructions; the original conductivity in the first row, traditional D-bar reconstructions in the second row and boundary corrected reconstructions in the third row; the numbers beside the pictures are L^2-errors, for the full error graph, see Figure 4. The first reconstruction pair is always calculated with $R = 3$, the second one is the one with the lowest numerical $\mathcal{L}^2$-error for the boundary corrected reconstruction, and the third one is with $R = 6$ to show how the reconstructions fail.

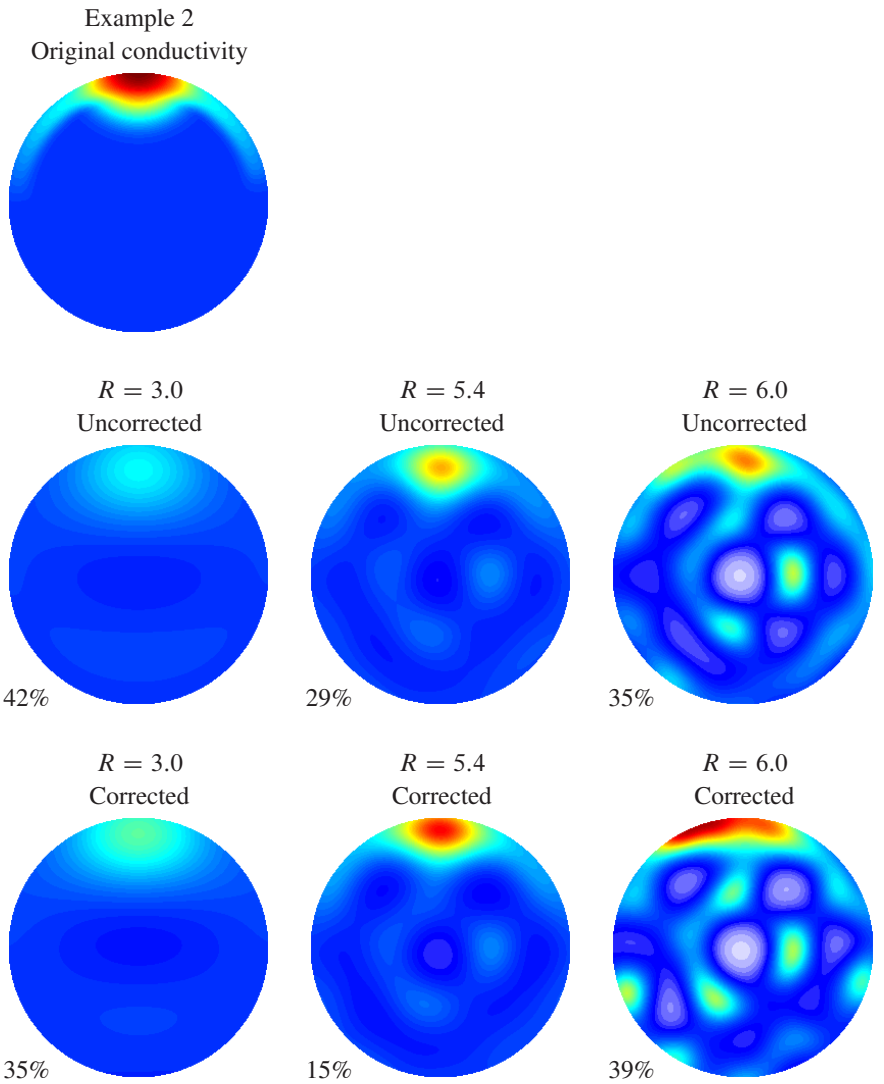

Figure 6. Example 2 reconstructions; the original conductivity in the first row, traditional D-bar reconstructions in the second row and boundary corrected reconstructions in the third row; the numbers beside the pictures are L^2-errors, for the full error graph, see Figure 4. The first reconstruction pair is always calculated with $R = 3$, the second one is the one with the lowest numerical $\mathcal{L}^2$-error for the boundary corrected reconstruction, and the third one is with $R = 6$ to show how the reconstructions fail.

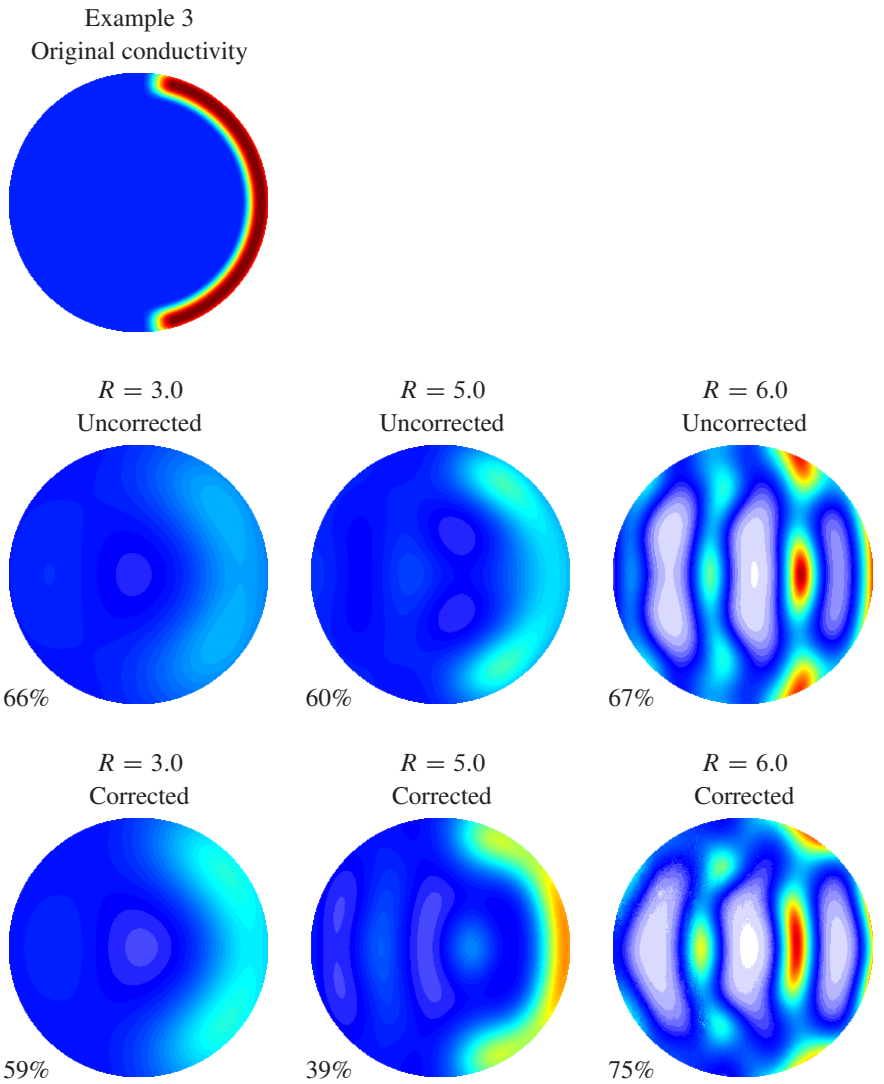

Figure 7. Example 3 reconstructions; the original conductivity in the first row, traditional D-bar reconstructions in the second row and boundary corrected reconstructions in the third row; the numbers beside the pictures are L^2-errors, for the full error graph, see Figure 4. The first reconstruction pair is always calculated with $R = 3$, the second one is the one with the lowest numerical $\mathcal{L}^2$-error for the boundary corrected reconstruction, and the third one is with $R = 6$ to show how the reconstructions fail.

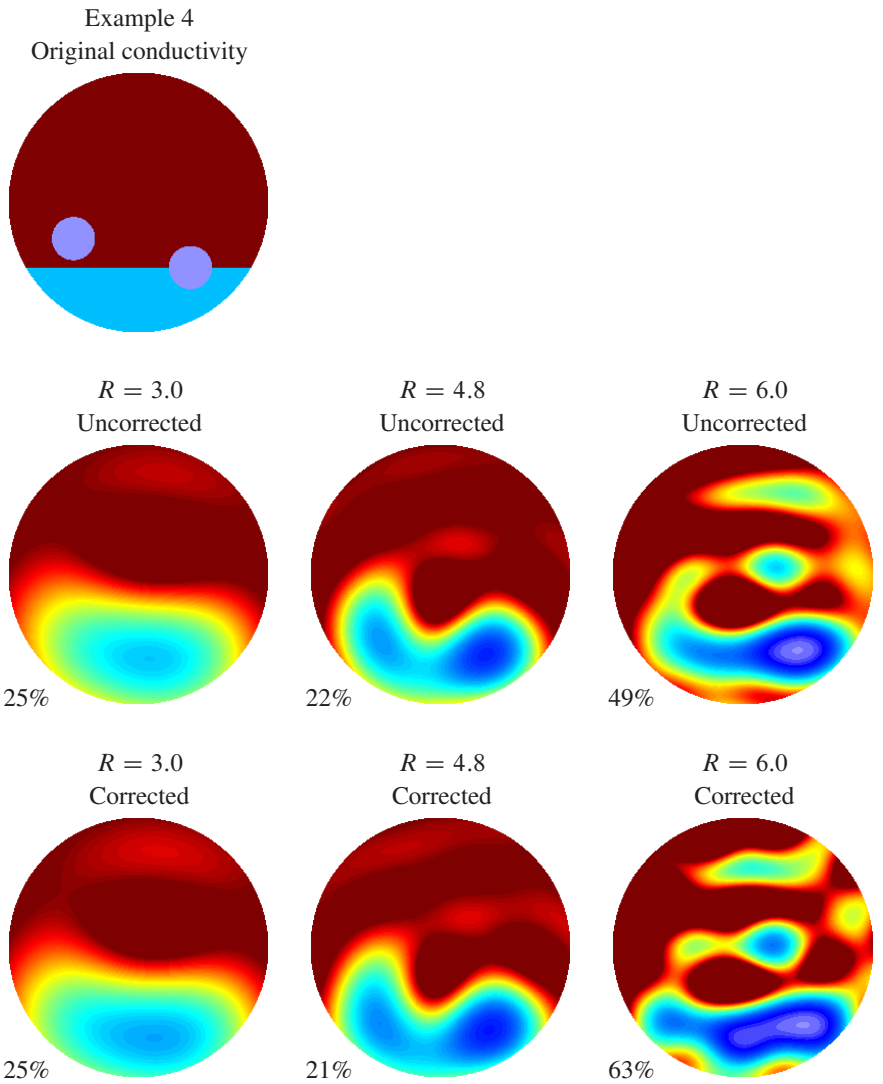

Figure 8. Example 4 reconstructions; the original conductivity in the first row, traditional D-bar reconstructions in the second row row and boundary corrected reconstructions in the third row; the numbers beside the pictures are L^2-errors, for the full error graph, see Figure 4. The first reconstruction pair is always calculated with $R = 3$, the second one is the one with the lowest numerical $\mathcal{L}^2$-error for the boundary corrected reconstruction, and the third one is with $R = 6$ to show how the reconstructions fail.

8 Conclusion

Our aim in this work is to find examples of simulated conductivities that (i) share features of conductivities appearing in applications of electrical impedance tomography, and (ii) allow higher-quality reconstruction when boundary correction step is added to the D-bar method. After experimenting with a large number of candidate conductivities we concluded that for conductivities which behave moderately at and near $\partial\Omega_1$, the method of approximating the trace of conductivity by an optimal constant is good enough. More precisely, the errors caused by measurement noise in Steps (a′) and (c′) prevented the boundary correction procedure from enhancing the reconstructions.

However, we were able to find several examples where the boundary corrected D-bar method does provide better imaging quality than the non-corrected method both in terms of quantitative error and visual inspection. Four such examples are presented in Section 7, and all of them have high contrast features in the conductivity right at the boundary. Consequently, most medical applications do not need the boundary correction procedure, but it may be beneficial or even necessary for some nondestructive testing, industrial process monitoring or geophysical sensing applications.

Acknowledgments. During part of the preparation of this work, S. Siltanen worked as professor and J. P. Tamminen worked as an assistant at the Department of Mathematics of Tampere University of Technology. The authors thank Jennifer Mueller for her valuable comments on the manuscript.

Bibliography

[1] K. Astala, J. L. Mueller, L. Päivärinta and S. Siltanen, Numerical computation of complex geometrical optics solutions to the conductivity equation, *Appl. Comput. Harmon. Anal.* **29** (2010), 2–17.

[2] K. Astala, J. L. Mueller, A. Perämäki, L. Päivärinta and S. Siltanen, Direct electrical impedance tomography for nonsmooth conductivities, *Inverse Probl. Imaging* **5** (2011), no. 3, 531–549.

[3] K. Astala and L. Päivärinta, A boundary integral equation for Calderón's inverse conductivity problem, *Collect. Math.* **2006** (2006), Spec. Issue, 127–139.

[4] K. Astala and L. Päivärinta, Calderón's inverse conductivity problem in the plane, *Ann. of Math. (2)* **163** (2006), 265–299.

[5] D. C. Barber and B. H. Brown, Applied potential tomography, *J. Phys. E. Sci. Instrum.* **17** (1984), 723–733.

[6] J. Bikowski, *Electrical impedance tomography reconstructions in two and three dimensions. From Calderón to direct methods*, Ph.D. thesis, Colorado State University, 2008.

[7] J. Bikowski, K. Knudsen and J. L. Mueller, Direct numerical reconstruction of conductivities in three dimensions using scattering transforms, *Inverse Problems* **27** (2011), 015002.

[8] J. Bikowski and J. L. Mueller, 2D EIT reconstructions using Calderon's method, *Inverse Probl. Imaging* **2** (2008), 43–61.

[9] L. Borcea, Electrical impedance tomography, *Inverse Problems* **18** (2002), R99–R136.

[10] L. Borcea, Addendum to electrical impedance tomography, *Inverse Problems* **19** (2003), 997–998.

[11] L. Borcea, V. Druskin and F. G. Vasquez, Electrical impedance tomography with resistor networks, *Inverse Problems* **24** (2008), 035013.

[12] G. Boverman, D. Isaacson, T.-J. Kao, G. J. Saulnier and J. C. Newell, Methods for direct image reconstruction for EIT in two and three dimensions, in: *Proceedings of the 2008 Electrical Impedance Tomography* (Hanover 2008), `http://engineering.dartmouth.edu/eit2008/EIT_Conference_2008.pdf`.

[13] R. M. Brown and G. Uhlmann, Uniqueness in the inverse conductivity problem for nonsmooth conductivities in two dimensions, *Comm. Partial Differential Equations* **22** (1997), 1009–1027.

[14] A. P. Calderón, On an inverse boundary value problem, in: *Seminar on Numerical Analysis and Its Applications to Continuum Physics*, Sociedade Brasileira de Matemàtica, Rio de Janeiro (1980), 65–73.

[15] M. Cheney and D. Isaacson, Distinguishability in impedance imaging, *IEEE Trans. Biomed. Eng.* **39** (1992), 852–860.

[16] M. Cheney, D. Isaacson and J. C. Newell, Electrical impedance tomography, *SIAM Rev.* **41** (1999), 85–101.

[17] M. Cheney, D. Isaacson, J. Newell, J. Goble and S. Simske, NOSER: An algorithm for solving the inverse conductivity problem, *Int. J. Imaging Syst. Technol.* **2** (1990), 66–75.

[18] R. D. Cook, G. J. Saulnier and J. C. Goble, A phase sensitive voltmeter for a high-speed, high-precision electrical impedance tomograph, in: *Engineering in Medicine and Biology Society. Vol. 13: 1991*, IEEE Press, New York (1991), 22–23.

[19] H. Cornean, K. Knudsen and S. Siltanen, Towards a D-bar reconstruction method for three-dimensional EIT, *J. Inverse Ill-Posed Probl.* **12** (2006), 111–134.

[20] D. C. Dobson, Convergence of a reconstruction method for the inverse conductivity problem, *SIAM J. Appl. Math.* **52** (1992), no. 2, 442–458.

[21] D. C. Dobson and F. Santosa, An image-enhancement technique for electrical impedance tomography, *Inverse Problems* **10** (1994), 317–334.

[22] L. D. Faddeev, Increasing solutions of the Schrödinger equation (in Russian), *Dokl. Akad Nauk SSSR* **165** (1965), 514–517; translation in *Sov. Phys. Dokl.* **10** (1966), 1033–1035.

[23] M. Ikehata and S. Siltanen, Numerical solution of the Cauchy problem for the stationary Schrödinger equation using Faddeev's Green function, *SIAM J. Appl. Math.* **64** (2004), 1907–1932.

[24] D. Isaacson, J. L. Mueller, J. C. Newell and S. Siltanen, Reconstructions of chest phantoms by the D-bar method for electrical impedance tomography, *IEEE Trans. Med. Imaging* **23** (2004), 821–828.

[25] D. Isaacson, J. L. Mueller, J. C. Newell and S. Siltanen, Imaging cardiac activity by the D-bar method for electrical impedance tomography, *Physiol. Meas.* **27** (2006), S43–S50.

[26] J. Kaipio, V. Kolehmainen, E. Somersalo and M. Vauhkonen, Statistical inversion and Monte Carlo sampling methods in electrical impedance tomography, *Inverse Problems* **16** (2000), 1487–1522.

[27] S. Kindermann and A. Leitão, Regularization by dynamic programming, *J. Inverse Ill-Posed Probl.* **15** (2007), no. 3, 295–310.

[28] K. Knudsen, *On the inverse conductivity problem*, Ph.D. thesis, Aalborg University, 2002.

[29] K. Knudsen, A new direct method for reconstructing isotropic conductivities in the plane, *Physiol. Meas.* **24** (2003), 391–401.

[30] K. Knudsen, M. J. Lassas, J. L. Mueller and S. Siltanen, D-bar method for electrical impedance tomography with discontinuous conductivities, *SIAM J. Appl. Math.* **67** (2007), 893–913.

[31] K. Knudsen, M. Lassas, J. L. Mueller and S. Siltanen, Reconstructions of piecewise constant conductivities by the D-bar method for electrical impedance tomography, *J. Phys. Conf. Ser.* **124** (2008), 012029.

[32] K. Knudsen, M. Lassas, J. L. Mueller and S. Siltanen, Regularized D-bar method for the inverse conductivity problem, *Inverse Probl. Imaging* **3** (2009), 599–624.

[33] K. Knudsen, J. L. Mueller and S. Siltanen, Numerical solution method for the D-bar-equation in the plane, *J. Comput. Phys.* **198** (2004), 500–517.

[34] K. Knudsen and A. Tamasan, Reconstruction of less regular conductivities in the plane, *Comm. Partial Differential Equations* **29** (2004), 361–381.

[35] V. Kolehmainen, M. Lassas and P. Ola, The inverse conductivity problem with an imperfectly known boundary, *SIAM J. Appl. Math.* **66** (2005), 365–383.

[36] V. Kolehmainen, M. Lassas and P. Ola, Electrical impedance tomography problem with inaccurately known boundary and contact impedances, *IEEE Trans. Med. Imaging* **27** (2008), 1404–1414.

[37] V. Kolehmainen, M. Lassas and P. Ola, Calderon's inverse conductivity problem with an imperfectly known boundary and reconstruction up to a conformal deformation, *SIAM J. Math. Anal.* **42** (2010), 1371–1381.

[38] A. Lechleiter and A. Rieder, Newton regularizations for impedance tomography: A numerical study, *Inverse Problems* **22** (2006), 1967–1987.

[39] J. L. Mueller and S. Siltanen, Direct reconstructions of conductivities from boundary measurements, *SIAM J. Sci. Comput.* **24** (2003), 1232–1266.

[40] E. K. Murphy, *2-D D-bar conductivity reconstructions on non-circular domains*, Doctoral thesis, Colorado State University, 2007.

[41] E. K. Murphy, J. L. Mueller and J. C. Newell, Reconstructions of conductive and insulating targets using the D-bar method on an elliptical domain, *Physiol. Meas.* **28** (2007), S101–S114.

[42] A. I. Nachman, Reconstructions from boundary measurements, *Ann. of Math. (2)* **128** (1988), 531–576.

[43] A. I. Nachman, Global uniqueness for a two-dimensional inverse boundary value problem, *Ann. of Math. (2)* **143** (1996), 71–96.

[44] G. Nakamura, K. Tanuma, S. Siltanen and S. Wang, Numerical recovery of conductivity at the boundary from the localized Dirichlet to Neumann map, *Computing* **75** (2005), 197–213.

[45] R. G. Novikov, A multidimensional inverse spectral problem for the equation $-\Delta\psi + (v(x) - Eu(x))\psi = 0$ (in Russian), *Funktsional. Anal. i Prilozhen.* **22** (1988), 11–22; translation in *Funct. Anal. Appl.* **22** (1988), 263–272.

[46] R. G. Novikov, On non-overdetermined inverse scattering at zero energy in three dimensions, *Ann. Sc. Norm. Super. Pisa Cl. Sci. (5)* **(5)** (2006), 279–328.

[47] R. G. Novikov, An effectivization of the global reconstruction in the Gel'fand–Calderon inverse problem in three dimensions, in: *Imaging Microstructures. Mathematical and Computational Challenges* (Paris 2008), Contemp. Math. 494, American Mathematical Society, Providence (2009), 161–184.

[48] R. G. Novikov and G. M. Khenkin, The d-bar equation in the multidimensional inverse scattering problem, *Uspekhi Mat. Nauk* **42** (1987), no. 2, 93–152.

[49] D. Roy, G. Nicholls and C. Fox, Imaging convex quadrilateral inclusions in uniform conductors from electrical boundary measurements, *Stat. Comput.* **19** (2009), 17–26.

[50] A. Seppänen, M. Vauhkonen, P. J. Vauhkonen, E. Somersalo and J. P. Kaipio, State estimation with fluid dynamical evolution models in process tomography – an application to impedance tomography, *Inverse Problems* **17** (2001), 467–483.

[51] H. Shan, M. V. Klibanov, H. Liu, N. Pantong and J. Su, Numerical implementation of the convexification algorithm for an optical diffusion tomograph, *Inverse Problems* **24** (2008), 025006.

[52] S. Siltanen, J. Mueller and D. Isaacson, An implementation of the reconstruction algorithm of A. Nachman for the 2-D inverse conductivity problem, *Inverse Problems* **16** (2000), 681–699.

[53] E. Somersalo, M. Cheney, D. Isaacson and E. Isaacson, Layer stripping: A direct numerical method for impedance imaging, *Inverse Problems* **7** (1991), 899–926.

[54] J. Sylvester, A convergent layer stripping algorithm for the radially symmetric impedance tomography problem, *Comm. Partial Differential Equations* **17** (1992), 1955–1994.

[55] J. Sylvester and G. Uhlmann, A global uniqueness theorem for an inverse boundary value problem, *Ann. of Math. (2)* **125** (1987), 153–169.

Received July 8, 2013.

Author information

Samuli Siltanen, Department of Mathematics and Statistics,
00014 University of Helsinki, Finland.
E-mail: samuli.siltanen@helsinki.fi

Janne P. Tamminen, Department of Mathematics and Statistics,
00014 University of Helsinki, Finland.
E-mail: janne.tamminen@helsinki.fi